Safe Navigation for Indoor Mobile Robots - Part II: Exploration, Self Localization and Map Building

Alessandro Corrêa Victorino, Patrick Rives, Jean-Jacques Borrelly

Abstract— **This paper is the second part of the author's contribution on the topic of *Safe Navigation for Indoor Mobile Robots*. It presents a new solution to the exploration, self localization and map building problem taking advantage of the sensor-based navigation framework presented in the paper: *Safe Navigation for Indoor Mobile Robots - Part I: A Sensor-based Navigation Framework*. The model of the indoor environment is structured as an hybrid representation, both topological and geometrical, which is incrementally built during the exploration task. The topological aspect of the model captures the connectivity and accessibility of the different places in the environment, and the geometrical model holds up an accurate robot localization and map building method. To overpass the problem of drift inherited to the odometry when the robot navigates in large scale environments, a new dead-reckoning method is proposed combining laser readings and feedback control inputs. Embedding the self-localization and map building problem in a sensor-based navigation framework improves both the quality and the robustness of the representation built during the exploration phase and authorizes a further use to achieve safe navigation tasks successfully. Experiments are shown which confirm the interests of the proposed methodology.**

I. Introduction

The sensor-based control methodology previoulsly published in the Part I of this work allows the robot to safely move into his whole free space using only the range measurements provided by a laser scanning device. However, it is well known that an efficient navigation strategy is not possible without an accurate robot localization and a reliable representation of the environment. The present paper focuses on these issues. We present here a precise localization methodology and a robust environment modeling, taking advantage of the sensor-based navigation strategy described in the Part I.

Many researches are currently done to provide robust solutions to the robot localization problem. A common conclusion is that due to the presence of drift and sliding, the odometry data from the wheel encoders (and more generally, the data provided by dead-reckoning methods) are frequently corrupted and not reliable enough to provide a correct long-dated estimate of the robot localization. So, it is essential to take into account the perception of the environment provided by robot's sensors in the localization process. Generally, when an a priori map of the environnement is available, the robot position is computed thanks to a matching technique applied between the currently observed part of the environment and the global a priori map. More recent methods of localization based on *Monte-Carlo simulation* are currently under investigation [22]. When no knowledge about the environment is assumed, it is necessary to solve two problems, localization and environment modeling, in a unique step, resulting that the representation of the environment and the robot positioning are mutually influenced by the uncertainties on the robot displacements. This problem is known as the *SLAM - simultaneous localization and mapping -* or so-called *CLM - concurrent localization and mapping -* problem. Different approaches are proposed depending on the nature of the representation, metric or topological, of the environement which is handled. Each type of representation brings advantages and drawbacks. Metric representations authorize a precise localization but are very sensitive to the propagation of uncertainties and drifts introduced by the dead-reckoning methods used to predict the robot motion during the exploration. Many instabilities and errors occur, mainly in large scale environments with cycles, when the distances navigated by the robot increase and, as a consequence, the quality of the metric mapping and localization process considerably decreases. In a topological description of the environment, the semantic or relational aspects (corridor intersections, door crossing, room A is connected to room B, etc.) are evaluated rather than the metric ones. It is well adapted to support a robust navigation in a large environment, however only a coarse localization based on the semantic aspects, can be performed.

In this context, we propose a new hybrid representation of the environment merging the advantages of metric and topological descriptions. A complete rep-

The authors are with the Institut National de Recherche en Informatique et en Automatique - INRIA-Sophia Antipolis(ICARE), address: 2004 Route des Lucioles BP 93 06902 Sophia Antipolis Cedex - France, E-mail: {FirstName.LastName}@sophia.inria.fr. Alessandro Corrêa Victorino is supported by a doctoral fellowship from the Coordenação de Aperfeiçoamento de Pessoal de Nível Superior - CAPES, Brazil, under Grant 2336/97-9.

resentation of the free space is incrementally built on-line lying on an exploration strategy. We show how this hybrid representation can be used to improve the localization of the robot in a large environment, either with respect to a precise metric representation of a given region of the environment or with respect to a global topological description of the environment.

The paper is organized as follows. Before introducing our environment modelling and robot localization methodology, we present a brief state of the art on the metric and topological representations in section II. In section III, we design the hybrid model mixing both topological and geometrical aspects for navigation purposes. It is shown that the structure of the topological model proceeds from the application of the sensor-based control strategy presented in Part I of this work. In section IV, we focus on the construction of the geometrical model, a motion estimator method is presented based on the telemetric laser measurements. Experimental results are discussed in section V and in section VI some conclusions and comments are presented.

II. State of the art

Metric representations have been developed in two broad approaches based either on an exact parametric description of the environment [8], [9], [17], [13], [10], or on a discrete cell decomposition [16], [14], [20]. In the first case, the model of the environment is constructed based on geometrical primitives describing the surface of the objects which are extracted and updated from the sensor observations. These maps are often referred on a fixed reference frame in the environment. In the second case, the environment is represented by a discrete grid where each cell is defined by a probability index that indicates if the cell is occupied by a obstacle or if it belongs to the free space. The probability index is updated using the sensor observations currently available and the a priori knowledge by means of a Bayesian rule.

In these approaches based on a geometric map, the robot holds a description of the borders of its free space that enables a metric localization with sufficient precision. This precision is essential for the execution of navigation tasks that require some degree of interaction between the robot and its environment. The principal restriction to the development of geometric approaches is the sensitivity of the localization and mapping algorithms with regard to the odometry errors integrated during the navigation. In almost cases, an important geometric distortion appears in the map when the distance covered by the robot increases. This distortion makes difficult the matching between the observations and the global map when the robot comes back in a place previously explored. Moreover, the geometric model is not appropriate to describe the topology and accessibility of the different places of the environment.

The topological approach is based on a partitioning of the environment in homogeneous areas (rooms, corridors, halls..) connected by links which represent the relations of accessibility [15], [12], [5]. In this representation, the semantic aspects are enhanced with regard to the metric aspects [6]. The topological model is generally a graph of nodes and edges: the nodes represent the explored areas or places, and the edges represent the way to access the different places from a given starting position in the environment. Navigation instructions or attributes are associated to the graph and dynamically explored during a navigation task. The attributes associated to the nodes (local structure of the environment, colors, etc.) are extracted from video or telemetric images and are generally related to the identification of a place and to the robot localization. The attributes associated to the edges, equally extracted from the sensor's observations, are used to enable the navigation between the different nodes, as the control decision aspects (turn on the right, go ahead...) or the reference trajectory to be followed [11], [23]. In [18] the topological model is built on-line during the exploration phase and results on the Voronoï diagram associated to the rigid environment. The attributes associated to the nodes are the features extracted from the telemetric measures corresponding to the characteristic places in the environment like doors or crossings of corridors.

The topological model captures the connectivity and the accessibility aspects, providing then a robust way to navigate from one place to another in a large environment. The localization of the robot is performed in a qualitative way based on the semantic relationship between the different places represented in the graph, limiting the application of this approach to the navigation tasks where a precise metric localization (that is provided in a geometric model) is not required.

These two modeling approaches, geometrical model and topological model, when used separately, are not sufficient to provide a precise and robust indoor mobile robot navigation. Then, some authors have introduced a navigation methodology based on a hybrid modeling of the environment mixing geometric and topological representations. In [6], [22], [2], the topological model is constructed based on a geometric model, generally an occupation grid representation built in a previous learning phase. In [15] and [7], the topological repre-

sentation is constructed on-line from the sensor's observation during the exploration phase, the geometric representation is constructed a posterior independently of the topological model. The advantage added by this independence between the two representations is that the errors on the geometric model, generally raised from odometry, are not propagated to the topological representation. In the opposite, the confidence in the topological representation of a given place is restricted without the local precision added by the geometric representation (important in the execution of some precise navigation tasks like parking).

We propose in this paper a modeling approach that combines the precision of a geometric model to the robustness of the navigation strategy provided by the topological representation. Our approach is in part based on a method presented by Kuipers in [15], in the sense that the topological description of the environment is constructed in an autonomous way lying on a sensor-based navigation strategy, and, in part based on the methodology presented by Choset in [7], in the sense that the robot is constrained to move on the Voronoï diagram of the environment during the exploration phase. As an improvement from these previous works, we propose the construction of the geometric and topological model simultaneously in an incremental way during the exploration of the environment, what allows us to avoid the problems raised from the independence between the two models.

III. A Hybrid Navigation Model: Topological and Geometrical

In the paper: *Safe Navigation for Indoor Mobile Robots - Part I: A Sensor-based Navigation Framework*, it was detailed a sensor-based navigation framework which allows the robot to safely move in an indoor environment with collision avoidance and to access in all the places belonging to the free space. This sensor-based navigation framework lies on three navigation functions which are designed based on the Voronoï diagram (VD) properties, figure 1:

- e_1, join the nearest Voronoï branch from any point of the free space and stabilize the robot on it,
- e_2, move along a Voronoï branch,
- e_3, stop the robot in a Voronoï bifurcation point (BP).

Moving along the VD branches represents a natural way to safely navigate between two different points of an indoor environment. Stopping in a BP is also useful for navigation purpose because the BPs are associated to the changes in the topology of the environment. The BPs are appropriate places both to localize the robot and to update the description of the environment. In this section, we present the different layers of the geometrical/topological representation which is incrementally built during the exploration of an indoor unknown environment.

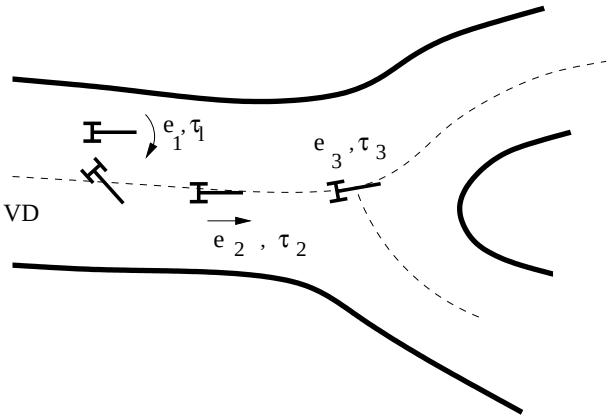

Fig. 1. *The navigation tasks. e_1, e_2 and e_3 are respectively the tasks of stabilization on a branch, stabilization and displacement along the branch and stabilization in a bifurcation point.*

A. The topological structure

Let us consider the figure 2. Applying the control methodology defined in the Part I, the navigation functions e_1, e_2 and e_3 are performed and the robot is constrained to travel on the VD of the unknown environment. During the exploration phase, the robot moves from the initial position marked by $BP11$, explores all the accessible free space passing through the places marked by *Place* 1, *Place* 2, *Place* 3 and *Place* 4, and come back to the position $BP11$ in figure 2. The robot travels on the VD of the environment without explicitly constructing it, the green trajectory is plotted for a better understanding only. We consider that the environment is static and the VD associated to this environment is unique.

By navigating on the VD of the environment in the example shown in figure 2, the robot constructs on-line a representation that determines the accessibility of its free space, and a relation between the different places of the environment established by the BPs connecting the branches. This topological representation is structured as shown in the figure 3, it is formed by a list of all the BPs found during the exploration. Each BP is registered on the list with a set of characteristics that describe the local topology of the environment, like the set of possible directions exiting it, the cross section of the local environment, and other geometric characteristics that are described in the next section. The possible directions exiting a BP are computed in the local frame based on the cross section of the local environment provided by the laser range finder at this

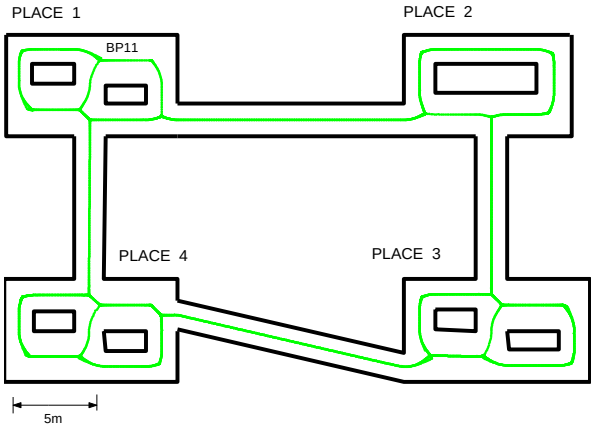

Fig. 2. Exploration of an indoor simulated environment.

position, and describes the connectivity of the environment. For example, when the robot exits $BP11$ by the direction $b1$, it arrives in the direction $b2$ of the $BP12$ in the *Place* 1. This topological structure is incrementally constructed during the exploration of the robot free space, and will be used further for achieving navigation tasks efficiently.

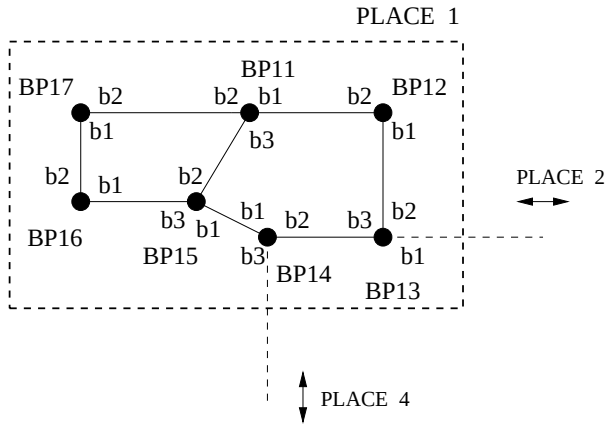

Fig. 3. A graph representation of the topological structure associated to the Place 1 of the environment shown in the figure 2

B. The geometrical structure

A geometrical representation is also incrementally built and updated during the navigation in parallel to the construction of the topological model [24]. The laser scanning device mounted on the robot delivers an horizontal cross section of the environment (figure 4).

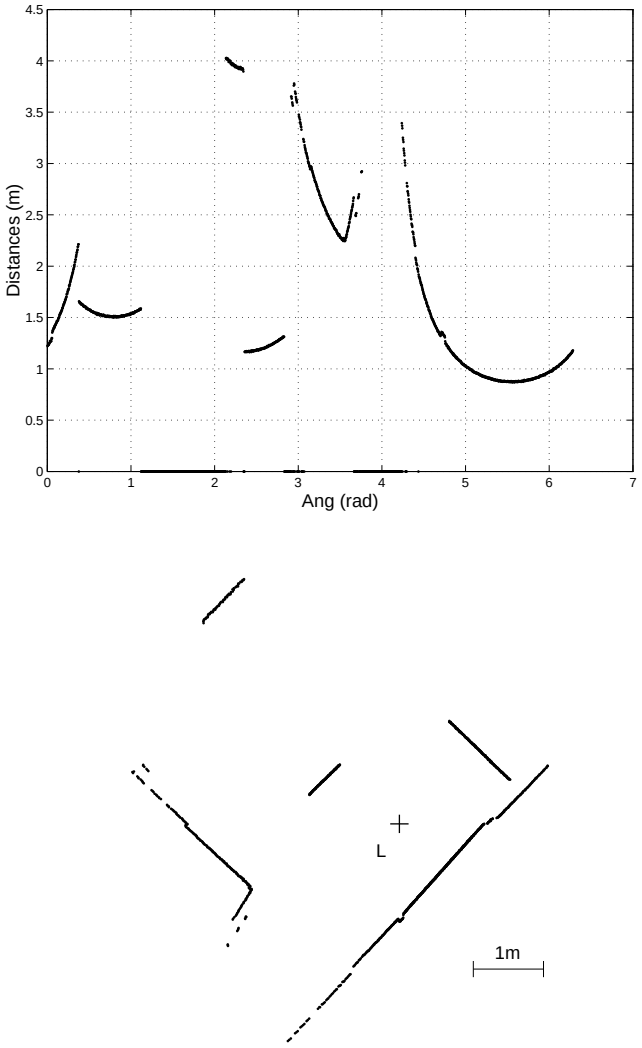

Fig. 4. *Cross section of the environment represented in the laser frame. Top: Polar representation, Bottom: Cartesian representation*

The simultaneous localization and map building methodology implemented is quite classic and already used by several authors. A coarse localization based on a dead reckoning technique is performed when the robot moves along the VD branches, and a map matching method based on a classical Extended Kalman Filter algorithm, is used when the robot stops on a BP.

However, in our case there are some improvements associated to the construction of the metric model:

- The motion of the robot is controlled with the execution of the three navigation tasks presented in section III during the exploration, that guarantees that the robot returns to a same physical place of the en-

vironment with a bounded error. As the Voronoï is unique for a given environment, it also guarantees a unique robot's trajectory will be realized in the real environment. Such a property notably enhances the localization and simultaneous map building process in a given place of the environment.
- The metric map of the place is updated and the robot position is corrected only when the robot stops in a BP of the Voronoï diagram. The main advantage of this approach is to perform a time consuming operation (i.e. updating the global map) only in the places associated to the changes in the topology of the environment.
- When the robot is moving on the branches, its position is estimated using the motion estimation method based on the laser measurements and detailed in section IV. In that way, the well-known problem of drift inherent to the use of a dead-reckoning method based on the wheels encoders, is considerably attenuated, as shown in the experimental results in section V.

These characteristics justify the use of a simplified version of the EKF [9], [3]. Recent versions more robust take into account cross-correlations in the covariances [17], [10]. More details on the implemented method can be found in the appendix A.

C. A hierarchical hybrid model of the environment

However, such a methodology shows some limitations when applied in large scale environments, as that shown in the example of the figure 2. Considering the figure 2, the robot leaves the region of the environment marked as *Place 1* and goes towards the first BP in the region indicated as *Place 2*. When it stops in this BP, the global map which was created when the robot was in *Place 1* should be updated following the SLAM strategy. In this case, due to the travel across the long corridor between the two places, it is not reasonable to refer the description of the *Place 2* on the initial reference frame fixed in *Place 1*. To solve this problem, we introduce a hierarchical representation of the environment where each place is described in its own local frame. The rule to decide when a new local frame (and a new place) must be initialized, is based on the capability, when the robot reaches a BP, to match the current local observation with the global map. Two cases can occur :

(a) There is a no empty set of segments which matches the local observation with the global map currently available. This fact indicates that the robot is still in a same *Place* of the environment and it enables the integration of the local observation updating the global map.

(b) The set of matches between the local observation and the global map is empty, due to the limited range of the laser. Then, a new reference frame is created in this position and a new map is initialized. This new reference frame characterizes a new *Place*. The relation with the previous place is essentially topological due to the uncertainties in the localization process during the travel.

In the resulting hybrid representation, the topological description captures the global accessibility while the geometrical one handles the local capabilities to reach a position precisely. The localization of the robot is performed at two levels:

(c) Qualitatively, thanks to the topological description, when the robot reaches a BP corresponding to a different place.

(d) Precisely, thanks to the metric representation, when the robot navigates in a peculiar place.

D. An example of SLAM

Let us consider the indoor environment shown in the figure 5. In this figure, the red robot corresponds to the current estimation of the robot position and the blue one is the real position with regard to the environment constrained by the sensor-based control laws. The blue crosses represent the absolute position in the initial reference frame, given by the odometry computed from the wheels encoders since the starting position without any map matching correction. The robot starts its exploration from the reference frame (figure 5-a). Using the e_1 and e_2 navigation functions, it reaches the branch of the VD and goes ahead until the first BP where it is stabilized thanks to the e_3 navigation function. From the laser scan, a set of line segments is extracted and the global map corresponding to the *Place* 1 is initialized. This map is defined in the reference frame. Then the robot goes towards a second BP (figure 5-a). Due to the short travel distance, a map matching technique can be used to merge the local laser scan with the global map in progress, updating then the geometrical description of the *Place* 1. Lying on this map matching, a precise localization of the robot can be done. The robot leaves the BP and navigates to the next one. Unfortunately, the presence of a long corridor prevents the matching between the local observation and the global map, and a new *Place* 2 is initialized with its own reference frame (figure 5-b). The *Places* 3, 4, 5 are successively created (figure 5-c and -d). Let us note that it is not possible to have a precise metric localization of *Places* 2, 3, 4, 5 (in construction) with respect to the initial reference frame attached to the *Place* 1. However each *Place* has its own precise metric model which are connected by the global topological graph.

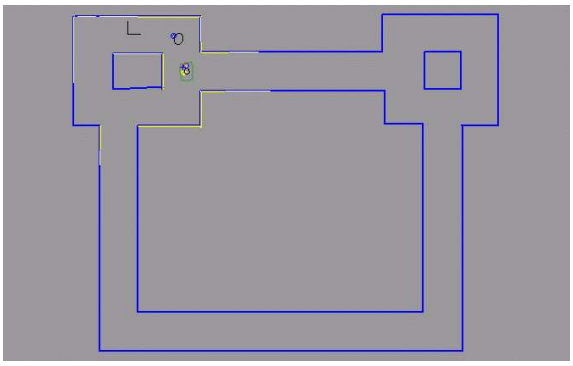

(a) Starting the exploration

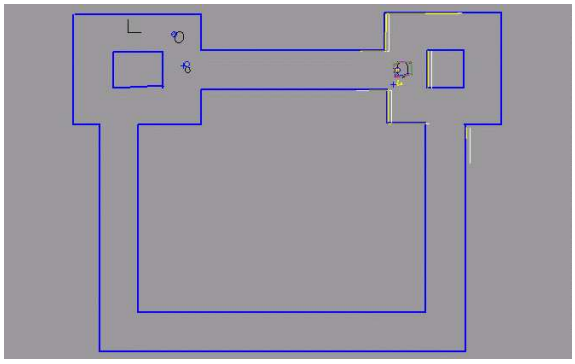

(b) Initializing the new place 2

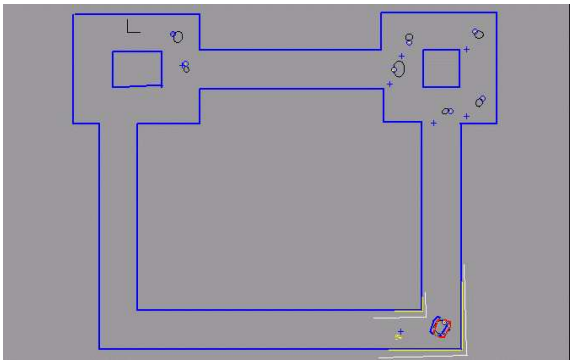

(c) Initializing the new place 3

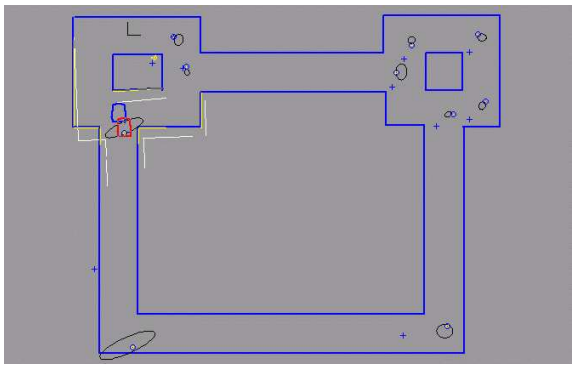

(d) Initializing the new place 5

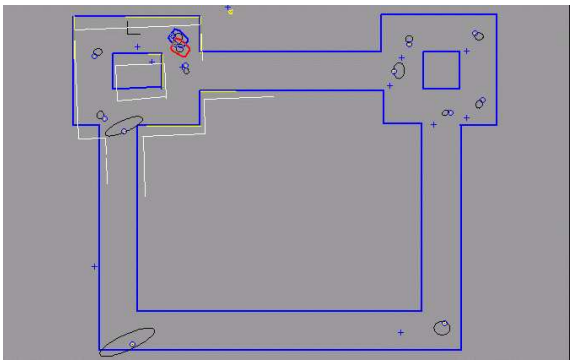

(e) Exploring the place 5

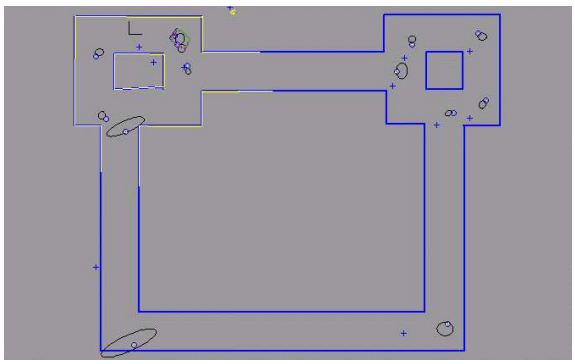

(f) Merging the places 1 and 5

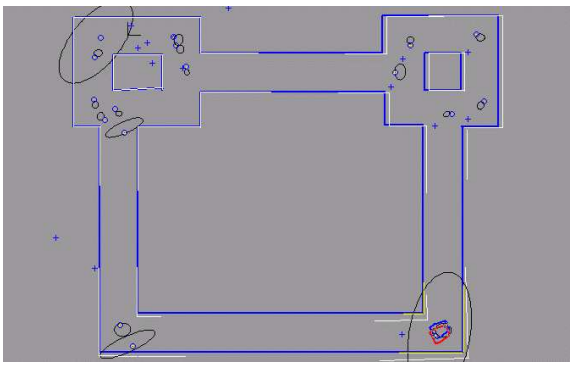

(g) Turning back to complete the exploration

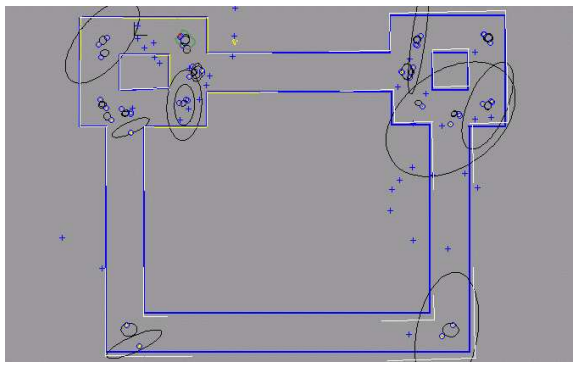

(h) Updating the global map by constraints propagation

Fig. 5. Exploration of an indoor environment.

In this sense, the "way to access" the *Places* is more relevant for the navigation task than the knowledge of a geometrical relation between them. A rough knowledge of the geometrical relation between two different *Places* must be assumed only in the case of cycles on the environment like in the situation shown in figure 5-e. The robot is mapping the *Place* 5 when it comes back in a BP which belongs to the (*Place* 1) already explored. Then the robot has to identify the revisited *Place* 1, to estimate its position in the metric model of *Place* 1, and to merge *Place* 1 and *Place* 5. This problem is considered in three aspects:

- *Place recognition*: As the robot is constrained to move on the VD due to the navigation tasks, the place recognition can be done by matching topological or geometrical local attributes (visual or telemetric local data) characteristic of the BP and stored in the global hybrid model of the environment. These aspects are not yet implemented in our experiments, so we assume that the recognition is possible only using a rough estimation of the robot position referred into the initial frame.

- *Estimation of the robot position w.r.t. the frame of a revisited place*: Figure 6 illustrates the situation corresponding to the figure 5-e. The local rigid transformations t_1 (Cartesian position of the revisited BP in the frame of *Place* 1) and t_5 (the current robot position in the frame of the *Place* 5) are approximatively known related to the uncertainties during the robot navigation. However, due to the bounded error of the sensor-based navigation and the property of the Voronï representation, we can ensure the BP reached by the robot when its navigates in the *Place* 1 and, after, when its navigates in the *Place* 5, corresponds to a same cartesian position in the physical world. The position of the robot in *Place* 1, t_x, is estimated by matching the local map observed in the robot frame with the global map of *Place* 1. The global map of *Place* 1 is projected into the robot frame using t_1 as prediction, then the rigid transformation, Δt, between the local map and the projected one is estimated using a bounded-error estimator presented in [26].

- *Fusion of places*: The transformation between the metric map of *Place* 1 and *Place* 5, t_{51}, is predicted with t_x and t_5. In order, t_{51} is estimated and the two metric maps are merged by the application of an extended Kalman filter approach, like that presented in [24].

Merging *Place* 1 and *Place* 5 allows to compensate the localization errors in the reference frame and the distortions in the global map using a backward propagation technique. This could be done by minimizing a cost function taking into account rigidity constraints

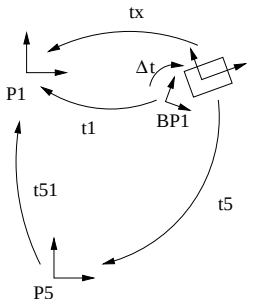

Fig. 6. A schematic representation of the situation shown in figure 5-e

inside a same place and elastic bands between two different places. After merging *Place* 1 and *Place* 5 the navigation continues by searching in the topological model the branches not completely explored (figure 5-f) . Finally, when the whole free space has been explored, the global map is updated as shown in the figure 5-g. The black ellipses (5 X magnified in the plot), illustrate the growth in the uncertainty and the drift in the localization during the travel when the positions are estimated uniquely from the odometry based on the wheels encoders .

Finally, using such a methodology, the geometrical model of the explored environment is segmented in different "Places", each one with a reference frame and an associated map where it is possible to localize the robot precisely. The access to the "Places" are defined in the topological graph associated to the Voronoï diagram as shown in the figure 3. The closed loop control laws designed in the Part-I of this work guarantee the tracking error along the Voronoï trajectory remains bounded. As the Voronoï is unique for a given environment, it also guarantees a unique robot's trajectory will be realized effectively. Such a property notably enhances the localization and simultaneous map building process in a given place of the environment. However, even if the trajectory following by the robot in the real physical world is well-defined and unique, its estimate built from the sensor measurements is subject to the drift inherent to the dead reckoning methods based on odometry provided by wheel encoders. So, when the distance covered by the robot between two different places becomes too large, problems can occur for detecting when the robot comes back to a previously observed place. We address this problem in the next section and we propose a new robust dead-reckoning method based only on the laser measurements in order to limit the influence of the drift during the displacement of the robot along the branches.

IV. A Robust Dead-reckoning Method based on Laser Range Data

In this section, we propose a new method for estimating the robot motion between two sampling times (k) and $(k+1)$ using the laser range data, (figure 7) and taking into account the uncertainties related to the perception process in a probabilistic framework. By this way, the method sounds like a dead-reckoning method which will be used in order to replace odometry based on wheel encoders during the displacement of the robot between two BPs. The relative motion is predicted in two stages [25] :

1. Assuming a local rigidity constraint on the environment, the robot motion can be estimated from two successive local laser scans, a first one at time (k) expressed into the frame Xc_k and another one at time $(k+1)$ expressed into the frame Xc_{k+1}, figure 7.
2. We use the knowledge on the control input provided by the sensor-based control laws to overpass the problem of incomplete observality detailed in section IV-A.1.

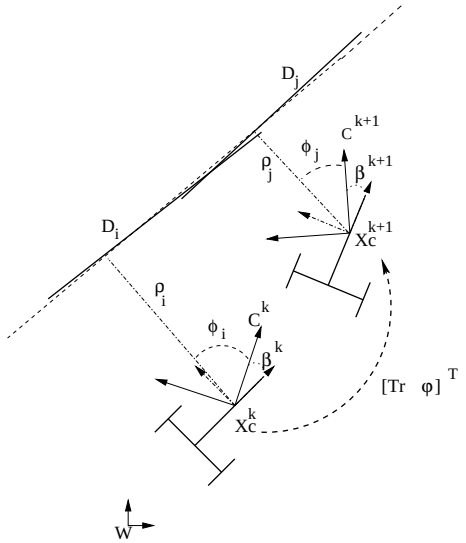

Fig. 7. The robot displacement $[Tr\ \varphi]^T$ between times (k) and $(k+1)$. C is the frame in which the control is computed. C has the orientation β with respect to a frame Xc fixed at the point x_c of the robot's basis. W is a fixed reference frame.

A. Estimating the robot displacement from two successive laser scans

The laser carried out by the robot periodically provides a planar scan of the local environment :

$$\{\delta(\theta_0), \ldots, \delta(\theta_i), \ldots, \delta(\theta_{2\pi})\} \tag{1}$$

where $\delta_i = \delta(\theta_i)$ is the distance from the origin of the laser frame to the nearest object at the angular position θ_i. A polar and Cartesian representation are shown in the figure 4.

The polar scan is segmented in a set of segments characterized by the ending points and the support lines. This set of segments computed in the laser frame at each time (k) represents the visible objects around the robot and it is called the local map I_k. Let us consider two local maps I_k and $I_{(k+1)}$ after the robot motion :

$$\begin{array}{rcl} I_k & = & \{D_0, \ldots, D_i, \ldots, D_n\}^k \\ I_{k+1} & = & \{D_0, \ldots, D_j, \ldots, D_m\}^{k+1} \end{array} \tag{2}$$

where:

$$\begin{array}{rcl} D_i & = & \{P_i, Q_i, \phi_i, \rho_i, \sigma^2_{\phi_i}, \sigma^2_{\rho_i}\} \\ D_j & = & \{P_j, Q_j, \phi_j, \rho_j, \sigma^2_{\phi_j}, \sigma^2_{\rho_j}\} \end{array}$$

- P and Q are the ending points of the segment.
- $(\phi, \rho, \sigma^2_\phi, \sigma^2_\rho)$ the parameters of the support line with their variances. D_i and D_j are represented in the laser frame at the times (k) and $(k+1)$ respectively, as shown in the figure 7.

A rigid transformation between I_k and I_{k+1} is defined as:

$$RT = \begin{pmatrix} T_x \\ T_y \\ \varphi \end{pmatrix} \tag{3}$$

The estimation of the displacement $[Tr\ \varphi]^T$ is equivalent to estimate the rigid transformation between I_k and $I_{(k+1)}$. That can be done by using a classical matching technique under the assumption that at least some segments in the two local maps correspond to the same objects of the environment.

Hypothesis 1: *There exists a set of objects $S \neq \emptyset$ in the environment which are observable from the positions Xc_k and Xc_{k+1}.*

The hypothesis 1 is necessary for the estimation of the rigid transformation (3) but not sufficient. In the next section, we demonstrate that, for some peculiar configurations of the environment, the rigid transformation RT is not fully observable from the laser range map.

A.1 The observability analysis

Let us consider the controlled frame C attached to the laser scanning device carried out by the robot (figure 7). Assuming nc lines can be perceived both at times (k) and $(k+1)$, and let us denote $SX_c = \{M_0 \ldots M_{nc}\}$ the set of these lines expressed in the controlled frame C at time (k). The state representation associated to the evolution of the controlled frame

C, in a continuous form, is given by:

$$\begin{cases} \dot{X}c = \mathcal{F}(Xc, U) & X_c \in \mathbb{R}^3 \\ Y = \mathcal{G}(Xc, \{M_0 \dots M_{nc}\}) & Y \in \mathbb{R}^{2nc} \end{cases} \quad (4)$$

where:
- $X_C = [x_c \ y_c \ \theta_c]^T$ is the state of C into the fixed reference frame.
- $U = [u_1 \ u_2 \ u_3]^T$ is the control input corresponding to the desired motion (τ_c in our case).
- $M_i = [\rho_i, \ \phi_i], \ i \in \{1, nc\}$ where ρ_i and ϕ_i are the parameters of the line i into a fixed frame in the environment. M_i is derived from the representation D_i (eq. 2)

The function $\mathcal{G}_{(2nc\times 1)}$ is the observation vector defined as,

$$\mathcal{G} = \begin{pmatrix} \rho_1 - x_c.cos(\phi_1) - y_c.sin(\phi_1) \\ \vdots \\ \rho_{nc} - x_c.cos(\phi_{nc}) - y_c.sin(\phi_{nc}) \\ \phi_1 - \theta_c \\ \vdots \\ \phi_{nc} - \theta_c \end{pmatrix} = \begin{pmatrix} g_1 \\ \vdots \\ g_{nc} \\ g_{nc+1} \\ \vdots \\ g_{2nc} \end{pmatrix}$$

The displacement $[Tr \ \varphi]^T$ results from the application of a control input τ_c computed from the laser measurements using the sensor-based control framework described in the Part-I of this work. The necessary condition required for the observability of $[Tr \ \varphi]^T$ from the range observations of the environment is stated in the Proposition 1.

Proposition 1: *Given a feedback control input τ_c which induces a relative motion $(k) \rightarrow (k+1)$ of the controlled frame, $[Tr \ \varphi]^T$, as shown in the figure 7 and given the set SX_c of matched lines in the local maps I_k and $I_{(k+1)}$, then $[Tr \ \varphi]^T$ is fully observable if there exists at least two lines $\{M_l, \ M_p\} \in SX_c$ so that,*

$$|\phi_l - \phi_p| \neq \pi$$

where ϕ_l and ϕ_p are the estimated orientation of the lines M_l and M_p into C_k. ∎

The proof holds on the well known result of *observability rank condition* for non-linear systems, [19], [3].

The observability rank condition states in a general case that,

Theorem 1: (*Observability rank condition*)
Let us consider a generalization of the system (4) with $\mathcal{F} : \mathbb{R}^n \rightarrow \mathbb{R}^n$ and $\mathcal{G} : \mathbb{R}^n \rightarrow \mathbb{R}^m$ where $\mathcal{G} = [\ g_1 \ g_2 \ \cdots \ g_m \ ]^T$. The observability matrix O *is written as:*

$$O = [\ dg_1 \ dL_f g_1 \ \cdots \ dL_f^{n-1} g_1 \ \cdots \ dg_m \ \cdots \ dL_f^{n-1} g_m \ ]$$

where

$$dg_i = [\frac{\partial g_i}{\partial X_{c1}} \ \cdots \frac{\partial g_i}{\partial X_{cn}}]^T$$

is the gradient of the i^{th} element of $\mathcal{G}$ with respect to X_c and

$$dL_f g = \frac{\partial g}{\partial X_c} f$$

and

$$dL_f^n g = \frac{\partial [dL_f^{n-1} g]}{\partial X_c}$$

are the Lie derivatives of g with respect to f.
If O is a full rank matrix then the system is locally observable. ∎

In a first step, the Proposition 1 is proved considering the particular case where only two lines are matched between I_k and $I_{(k+1)}$ (figure 8), then, the proof is generalized to the case of nc matches.

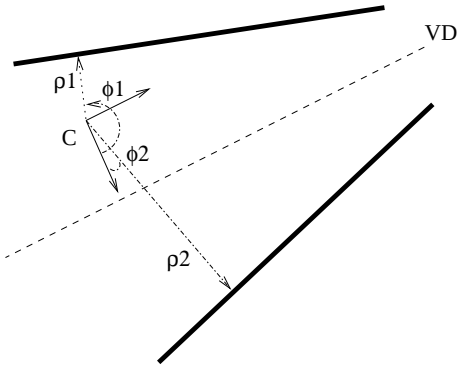

Fig. 8. Robot navigation in a corridor-like environment

Proof of the Proposition 1:

The observability matrix for the system in (4) in the case of two lines ($nc = 2$), is given by,

$$O_{(3\times 12)} = [\ dg_1 \ \ dg_2 \ \ dg_3 \ \ dg_4 \ \ dL_f g_1 \ \ dL_f g_2 \ \ dL_f g_3 \ \ dL_f g_4 \ \ dL_f^2 g_1 \ \ dL_f^2 g_2 \ \ dL_f^2 g_3 \ \ dL_f^2 g_4 \ ]$$

denoting $s_i = sin(\phi_i)$, $c_i = cos(\phi_i)$, $s_{ic} = sin(\phi_i - \theta_c)$ and $c_{ic} = cos(\phi_i - \theta_c)$ yields,

$$O_{(3\times 12)} = \begin{bmatrix} -c_1 & -c_2 & 0 & 0 & 0 & 0 & 0 & 0 & 0 & 0 & 0 & 0 \\ -s_1 & -s_2 & 0 & 0 & 0 & 0 & 0 & 0 & 0 & 0 & 0 & 0 \\ 0 & 0 & -1 & -1 & u_1 s_{1c} + u_2 c_{1c} & 0 & 0 & 0 & 0 & 0 & 0 & 0 \\ 0 & 0 & 0 & 0 & 0 & 0 & 0 & 0 & 0 & 0 & 0 & 0 \\ 0 & 0 & 0 & 0 & 0 & 0 & 0 & 0 & 0 & 0 & 0 & 0 \\ u_1 s_{2c} + u_2 c_{2c} & 0 & 0 & u_3[-u_1 c_{1c} + u_2 s_{1c}] & 0 & 0 & 0 & 0 & 0 & 0 & 0 & 0 \\ & & & & 0 & 0 & 0 & 0 & 0 & 0 & 0 & 0 \\ & & & & 0 & 0 & 0 & 0 & 0 & 0 & 0 & 0 \\ & & & & u_3[-u_1 c_{2c} + u_2 s_{2c}] & 0 & 0 & 0 & 0 & 0 & 0 & 0 \end{bmatrix}$$

Therefore $\forall \tau_c$ the rank of $O_{(3\times 12)}$ written above is the rank of the following sub-matrix $O'_{(3\times 3)}$

$$O' = \begin{bmatrix} -cos(\phi_1) & -cos(\phi_2) & 0 \\ -sin(\phi_1) & -sin(\phi_2) & 0 \\ 0 & 0 & -1 \end{bmatrix}$$

that is full rank if

$$|\phi_1 - \phi_2| \neq \pi$$

Let us consider the generalized system of (4), the ($nc > 2$) matches of the set SX_c are considered and the sub-matrix O' is rewritten in a general form as,

$$O' = \begin{bmatrix} -cos(\phi_1) & -cos(\phi_2) & \cdots & -cos(\phi_l) & \cdots \\ -sin(\phi_1) & -sin(\phi_2) & \cdots & -sin(\phi_l) & \cdots \\ 0 & 0 & \cdots & 0 & \cdots \\ -cos(\phi_p) & \cdots & -cos(\phi_{nc}) & 0 & \\ -sin(\phi_p) & \cdots & -sin(\phi_{nc}) & 0 & \\ 0 & \cdots & 0 & -1 & \end{bmatrix}$$

Therefore, if there exists at least a couple of matched lines $\{M_l,\ M_p\} \in SX_c$ so that

$$|\phi_l - \phi_p| \neq \pi$$

it will always exist a full rank sub-matrix O'' of O' and the generalized system of (4) is observable. ∎

Finally, assuming that the rigid transformation (3) is fully observable, then the property (1) can be stated.

Property 1: *Given $\{I_k, I_{k+1}, S_l \in I_k, S_m \in I_{k+1}\}$, then $\forall\ D_i \in S_l\ \exists\ D_j \in S_m$, so that, $D_i \overset{RT}{\rightarrow} D_j$. S_l and S_m are the representation of S at the times (k) and $(k+1)$.*

The property (1) will be used to estimate the rigid transformation (3). This rigid transformation is estimated in three steps :
1. the matching step (section IV-A.2),
2. the estimation of the rotation φ (section IV-A.3),
3. the estimation of the translation $Tr = [T_x\ T_y]^T$ (section IV-A.4).

A.2 The matching step

Given the two local maps I_k and I_{k+1}, (2), the correspondence between the segments is performed using a vote method. Initially the set of all *reasonable*[1] correspondence hypotheses between I_k and I_{k+1} are generated:

$$\mathcal{H} = \{(H_1, \ldots, H_h, \ldots, H_{NC})/H_h : D_i^k \overset{cor}{\rightarrow} D_j^{k+1}\} \quad (5)$$

[1]The elements of the maps are ordered and the displacement is small then an element i from I_k is supposed to have a correspondent in a neighborhood of the position i in I_{k+1}

where NC is the number of possible hypotheses to be evaluated, $D_i^k \overset{cor}{\rightarrow} D_j^{k+1}$ indicates that possibly there is a correspondence between the element i of I_k and the element j of I_{k+1}, that constitutes the hypothesis H_h.

Let us consider an element $H_h : D_i^k \overset{cor}{\rightarrow} D_j^{k+1}$ from $\mathcal{H}$. If this hypothesis is true then the robot (sensor) has been rotated of $\varphi_{ij} = \phi_j - \phi_i$, where $\phi_i \in D_i^k$ and $\phi_j \in D_j^{k+1}$. The rotation φ_{ij} is used to check the hypothesis thanks to the following algorithm:

$\forall\ D_l \in I_k$ if $\exists\ D_p \in I_{k+1}$
so that $(\phi_p + \varphi_{ij}) < \xi_{ijp}$, then
$Ac(H_h) = Ac(H_h) + 1$
$\{D_l^k\ , D_p^{k+1}\}$ is included in a set SC_h of all the correspondences under the hypothesis H_h.

where:
- $l \in \{1, \ldots, n\} - \{i\}$
- $p \in \{1, \ldots, m\} - \{j\}$
- $Ac(H_h)$ is the score of the hypothesis H_h.
- ξ_{ijp} is a function of the uncertainties associated with the measurements D_i^k, D_j^{k+1} and D_p^{k+1}.

After the application of this procedure to the set $\mathcal{H}$, the best hypothesis in $\mathcal{H}$ is selected as:

$$H^* = \max_{H_h \in \mathcal{H}} \{Ac(H_h)\} \quad (6)$$

Then the best correspondence between the local maps I_k and I_{k+1} is the set of couples of segments SC_{h^*} according to the best hypothesis H^*. SC_{h^*} is represented as:

$$\begin{cases} SC_{h^*} = \{sc_1, \ldots, sc_l, \ldots, sc_{nc}\} \\ sc_l = \{\Delta\phi_{ij}\ , \Delta\rho_{ij}\ , \sigma^2_{\Delta\phi_{ij}}\ , \sigma^2_{\Delta\rho_{ij}}\} \end{cases} \quad (7)$$

where,

- nc is the number of elements in SC_{h^*}.
- $\Delta\phi_{ij} = \phi_j - \phi_i$; $\phi_i \in D_i^k$ and $\phi_j \in D_j^{k+1}$
- $\Delta\rho_{ij} = \rho_j - \rho_i$; $\rho_i \in D_i^k$ and $\rho_j \in D_j^{k+1}$
- $\sigma^2_{\Delta\phi_{ij}} = \sigma^2_{\phi_i} + \sigma^2_{\phi_j}$; $\sigma^2_{\phi_i} \in D_i^k$ and $\sigma^2_{\phi_j} \in D_j^{k+1}$
- $\sigma^2_{\Delta\rho_{ij}} = \sigma^2_{\rho_i} + \sigma^2_{\rho_j}$; $\sigma^2_{\rho_i} \in D_i^k$ and $\sigma^2_{\rho_j} \in D_j^{k+1}$

The prediction of RT in (3), called $\hat{T}_L = [\hat{T}r_L\ \hat{\varphi}_L]^T$ is estimated taken into account the correspondences SC_h^*. A probabilistic framework is used to estimate $\hat{T}_L$ due to the noisy nature of the laser measurements.

A.3 The estimation of the rotation

Let us φ be the relative rotation of the sensor between the times (k) and $(k+1)$, φ is considered as a random variable with a normal distribution. The set,

$$\varphi \sim \{\Delta\phi_0, \ldots, \Delta\phi_l, \ldots, \Delta\phi_{nc}\} \quad (8)$$

resulted from the correspondence procedure is a sequence of measurements or realizations of φ. The estimate $\hat{\varphi}$ of φ is calculated using a *Maximum a Posteriori (MAP)* estimator.

Let us the measurement $\Delta\phi_0 = \varphi + e_0$ be a first realization of φ, where $e_0 \sim \mathcal{N}(0, \sigma^2_{\Delta\phi_0})$. An *a priori* distribution of φ is initialized as,

$$f(\varphi|\Delta\phi_0) = \mathcal{N}(\hat{\varphi}_0, \sigma^2_{\hat{\varphi}_0}) \tag{9}$$

where $\hat{\varphi}_0 = \Delta\phi_0$ and $\sigma^2_{\hat{\varphi}_0} = \sigma^2_{\Delta\phi_0}$.

Considering a measurement $\Delta\phi_l = \varphi + e_l$, $e_l \sim \mathcal{N}(0, \sigma^2_{\Delta\phi_l})$, in (8), the estimate $\hat{\varphi}_l$ after the realization $\Delta\phi_l$ is given by the maximization of the *a posteriori* distribution $f(\varphi|\Delta\phi_l)$,

$$\hat{\varphi}_l = \max_{\varphi}\{f(\varphi_l|\Delta\phi_l)\} \tag{10}$$

The a posteriori $f(\varphi|\Delta\phi_l)$ is determined following the Bayes rule,

$$\begin{array}{l} f(\varphi|\Delta\phi_l) = \frac{f(\varphi|\Delta\phi_{l-1})f(\Delta\phi_{l-1}|\varphi)}{f(\Delta\phi_{l-1})} \\ = c(\Delta\phi_{l-1})exp(-\frac{(\Delta\phi_{l-1}-\varphi)^2}{2\sigma^2_{\Delta\phi_l}} - \frac{\hat{\varphi}_{l-1}-\varphi}{2\sigma^2_{\hat{\varphi}_{l-1}}}) \end{array} \tag{11}$$

$c(\Delta\phi_{l-1})$ is not dependent of φ and can be dropped in the maximization. Then,

$$\begin{array}{rcl} \hat{\varphi}_l & = & \max_{\varphi}\{f(\varphi_l|\Delta\phi_l)\} \\ & = & \min_{\varphi}\{-\frac{(\Delta\phi_{l-1}-\varphi)^2}{2\sigma^2_{\Delta\phi_l}} - \frac{\hat{\varphi}_{l-1}-\varphi}{2\sigma^2_{\hat{\varphi}_{l-1}}}\} \end{array} \tag{12}$$

that is,

$$\hat{\varphi}_l = \hat{\varphi}_{l-1} + \frac{\sigma^2_{\hat{\varphi}_{l-1}}}{\sigma^2_{\hat{\varphi}_{l-1}} + \sigma^2_{\Delta\phi_l}}(\Delta\phi_l - \hat{\varphi}_{l-1}) \tag{13}$$

and,

$$\sigma^2_{\hat{\varphi}_l} = \frac{\sigma^2_{\hat{\varphi}_{l-1}}\sigma^2_{\Delta\phi_l}}{\sigma^2_{\hat{\varphi}_{l-1}} + \sigma^2_{\Delta\phi_l}} \tag{14}$$

The estimated rotation $\hat{\varphi}_L$ and its variance $\sigma^2_{\hat{\varphi}_L}$ are computed applying the equations (13) and (14) for all l in the sequence (8).

A.4 The estimation of the translation Tr

The translation between the local maps I_k and I_{k+1} is estimated using a weighted least square estimator based on the matching set SC_{h^*}. Let us consider the l^{th} element of SC_{h^*}, (7) in subsection IV-A.2, as:

$$sc_l = \{\Delta\phi_{ij}\ , \Delta\rho_{ij}\ , \sigma^2_{\Delta\phi_{ij}}\ , \sigma^2_{\Delta\rho_{ij}}\} \tag{15}$$

The translation $Tr = [T_x\ T_y]^T$, defined in (3), is related with the measurements in sc_l by the following error function:

$$e_l = A_l Tr - \Delta\rho_{ij_l} \tag{16}$$

where:

- The error e_l models the uncertainties related to the measurements.
- $A_l = \left[\ \cos(\phi_l^*) \quad \sin(\phi_l^*)\ \right]$
- ϕ_l^* is a mean value between the parameter ϕ_i and $(\phi_j + \hat{\varphi}_L)$.
- $\hat{\varphi}_L$ is the predicted rotation of the sensor frame calculated in (13).
- The variance of ϕ_l^* is given by $\sigma^2_{\phi_l^*} = \sigma^2_{\phi_i} + \sigma^2_{\phi_j} + \sigma^2_{\hat{\varphi}_L}$.
- $\Delta\rho_{ij_l}$ is as defined in (7).

Let us define a cost function J,

$$J = \sum_{l=1}^{nc} \mu_l e_l^T e_l \tag{17}$$

where μ_l is a weight determined in the matching step for handling the uncertainties in sc_l due to the measurement process.

The prediction of the relative translation Tr given by the laser measurement, $\hat{Tr}_L$, is then derived by minimizing (17):

$$\begin{array}{rcl} \hat{Tr}_L & = & \min_{Tr}\{\sum_{l=1}^{nc} \mu_l e_l^T e_l\} \\ & = & (\sum_{l=1}^{nc} \mu_l A_l^T A_l)^{-1} \sum_{l=1}^{nc} \mu_l A_l^T \Delta\rho_{ij_l} \end{array} \tag{18}$$

The covariance associated to $\hat{Tr}_L$ is calculated by propagating the uncertainties from the laser readings in sc_l, (7), to the predicted translation $\hat{Tr}_L$. The propagation of covariances between random frames was formalized in [21].

Let us define a function g from the minimization process,

$$\begin{array}{rcl} g & = & \frac{\partial J}{\partial Tr} \\ & = & \sum_{l=1}^{nc} \mu_l (A_l^T A_l Tr - A_l^T \Delta\rho_{ij_l}) \\ & = & \sum_{l=1}^{nc} f(Tr, M_l) \end{array} \tag{19}$$

where

$$M_l = \left[\ \phi_l^* \quad \Delta\rho_{ij_l}\ \right]^T$$

is a measurement vector.

Expanding (19) in Taylor series and taking the first order elements,

$$\begin{array}{rcl} g - g|_{(\hat{Tr}_L, \hat{M}_l)} & = & \sum_{l=1}^{nc} \mu_l \frac{\partial f}{\partial Tr}|_{(\hat{Tr}_L, \hat{M}_l)} \Delta Tr + \\ & & \sum_{l=1}^{nc} \mu_l \frac{\partial f}{\partial M_l}|_{(\hat{Tr}_L, \hat{M}_l)} \Delta M_l \end{array} \tag{20}$$

$g - g|_{(\hat{Tr}_L, \hat{M}_l)} \to 0$ since $\hat{Tr}_L$ minimizes (19). Then,

$$\begin{array}{rcl} 0 & = & (\sum_{l=1}^{nc} \mu_l \frac{\partial f}{\partial Tr}|_{(\hat{Tr}_L, \hat{M}_l)}) \Delta Tr + \\ & & \sum_{l=1}^{nc} \mu_l \frac{\partial f}{\partial M_l}|_{(\hat{Tr}_L, \hat{M}_l)} \Delta M_l \end{array} \tag{21}$$

As $\hat{Tr}_L$ is a minimum value of the quadratic function (17), the matrix

$$\frac{\partial g}{\partial Tr}|_{(\hat{Tr}_L,\hat{M}_l)} = \sum_{l=1}^{nc} \mu_l \frac{\partial f}{\partial Tr}|_{(\hat{Tr}_L,\hat{M}_l)} \quad (22)$$

must be definite positive and non singular so that the inverse matrix $(\sum_{l=1}^{nc} \mu_l \frac{\partial f}{\partial Tr}|_{(\hat{Tr}_L,\hat{M}_l)})^{-1}$ exists, it follows from (21),

$$\Delta Tr = -(\sum_{l=1}^{nc} a_l)^{-1} \sum_{l=1}^{nc} p_l \Delta M_l \quad (23)$$

where:

$$\begin{aligned} a_l &= \mu_l \frac{\partial f}{\partial Tr}|_{(\hat{Tr}_L,\hat{M}_l)} \\ p_l &= \mu_l \frac{\partial f}{\partial M_l}|_{(\hat{Tr}_L,\hat{M}_l)} \end{aligned}$$

Taking the expectations of (23),

$$\begin{aligned} &C_{\hat{Tr}_L} = E[\Delta Tr \Delta Tr^T] = \\ &(\sum_{l=1}^{nc} a_l)^{-1} \sum_{l=1}^{nc} \{p_l C_{M_l} p_l^T\} (\sum_{l=1}^{nc} a_l)^{-T} \end{aligned} \quad (24)$$

where:

$$C_{M_l} = \begin{bmatrix} \sigma^2_{\phi_l^*} & 0 \\ 0 & \sigma^2_{\Delta\rho_{ijl}} \end{bmatrix}$$

is the covariance of the measurements in sc_l. The development of (24) is given in the Appendix B.

To summarize, the prediction of the relative motion Tr is computed from the laser readings as

$$\hat{Tr}_L = (\sum_{l=1}^{nc} \mu_l A_l^T A_l)^{-1} \sum_{l=1}^{nc} \mu_l A_l^T \Delta\rho_{ijl} \quad (25)$$

with the covariance $C_{\hat{Tr}_L}$ computed in (24). In [4] a weighted least square method is also used in the estimation of the robot relative translation in a similar way.

If the Proposition 1 stated in the section IV-A.1 is not satisfied then the matrix

$$\sum_{l=1}^{nc} \mu_l A_l^T A_l$$

will be singular and the displacement cannot be observed anymore from the laser readings. This non-observability problem can be overpassed considering the odometry data from the wheels to complete the observation of the system.

Let us consider the equation (25). The estimated translation $\hat{Tr}_L$ is computed from the matching set SC_h in (7). A simple way to take advantage of the odometry observation in the computation of (25), is to extend the matching set SC_h by adding a *virtual* correspondence element $sc_{(nc+1)}$ built from the projection of the odometry measurement in the non-observed dimension of (25). Then $\hat{Tr}_L$ is computed by,

$$\hat{T}_L = (\sum_{l=1}^{nc+1} \mu_l A_l^T A_l)^{-1} \sum_{l=1}^{nc+1} \mu_l A_l^T \Delta\rho_{ijl} \quad (26)$$

where :
- ϕ_{nc+1} in A_{nc+1} is the non-observed direction of (25) into the frame L_k.
- $\Delta\rho_{ij_{nc+1}}$ is the projection of the odometry measurement onto the non-observed direction of (25).

B. Estimating the robot displacement from the desired control inputs

In this section, we define another motion estimator between two sampling times (k) and $(k+1)$, figure 7, by integrating the desired velocity control inputs. Then, this estimation will be merged with the prediction $\hat{T}_L$ computed in (24)-(26) from the laser readings. Using two concurrent ways for estimating the robot displacement provides more robustness and the possibility of detecting non systematic errors due to the slippage of the wheels or due to spurious sensor data .

Sensor-based control laws are derived so that the robot is constrained to move on the Voronoï diagram (VD) (figure 1 see *Safe Navigation for Indoor Mobile Robots - Part I: A Sensor-based Navigation Framework* for more details). The desired control input τ_C computed when the robot is moving on a Voronoï branch can be rewritten as:

$$\begin{aligned} \tau_C &= -\lambda e_{branch} + B\frac{\partial g_s}{\partial t} \\ e_{branch} &= Ae_1 + Bg_s \end{aligned} \quad (27)$$

The desired control input τ_C when the robot is stabilized at a bifurcation point can be rewritten as,

$$\begin{aligned} \tau_C &= -\lambda e_{BP} \\ e_{BP} &= Ce_3 \end{aligned} \quad (28)$$

where:
- τ_C is the velocity control input expressed into the frame C_k,(figure 7).
- e_1 (two dimensional) and e_3 (three dimensional) are respectively the output errors corresponding to the stabilization on a branch and on a BP; they are depending on the distance and orientation computed from the laser readings.
- g_s is a secondary task which allows to move ahead the robot along the branch, let us note that the subspace spanned by this secondary task is orthogonal to the subspace spanned by e_1.

- e_{branch} is an hybrid task grouping e_1 and g_s.
- e_{BP} is an hybrid task proportional to e_3.
- We assume the laser readings and the variables τ_C, e_1, e_3, g_s, e_{branch} and e_{BP} have random distribution.
- $A_{(3\times2)}$, $B_{(3\times3)}$ and $C_{(3\times3)}$ are constant not random matrices.

The control τ_C, calculated from equations (27) and (28) at each time (k), is a velocity input $\tau_C = \begin{bmatrix} v_x & v_y & \dot{\theta}_C \end{bmatrix}^T$ where v_x and v_y are the desired translational velocities and $\dot{\theta}_C$ the desired rotational velocity of the frame C in the fixed frame W, figure 7. With the application of τ_C the robot moves to a new position at the time $(k+1)$. The objective is to compute a prediction, and the associated uncertainty, of this motion based on the integration of τ_C. τ_C is computed in the controlled frame (C), (figure 7).

Let us consider the motion of the frame C under the control τ_C,

$$\Delta X_C = \tau_C \Delta t + \nu \tag{29}$$

where:

- ΔX_C and τ_C are expressed in the frame C_k.
- Δt is the sampling rate of the feedback control loop.
- ν is the error on the realization of τ_C.

Two sources of uncertainties are identified from the model (29):

- The uncertainties associated with laser readings which corrupt the computation of τ_C.
- The uncertainties associated with the impossibility of the complete realization of τ_C by the real dynamic system. These uncertainties are related with the modeling errors of the robot and the eventual slippage of the wheels.

The predicted motion of the controlled frame C is given by,

$$\Delta \hat{X}_C = \begin{bmatrix} \Delta \hat{x}_C \\ \Delta \hat{y}_C \\ \Delta \hat{\theta}_C \end{bmatrix} = \hat{\tau}_C \Delta t \tag{30}$$

The variance is derived taking the expectations of the prediction error,

$$\begin{array}{rcl} P_{\Delta \hat{X}_C} & = & E[(\Delta X_C - \Delta \hat{X}_C)(\Delta X_C - \Delta \hat{X}_C)^T] \\ P_{\Delta \hat{X}_C} & = & \Delta t^2 Q_C + Q_m \end{array} \tag{31}$$

where:

- $Q_C = E[(\tau_C - \hat{\tau_C})(\tau_C - \hat{\tau_C})^T]$ is the covariance of the control τ_C.
- $Q_m = E[\nu\nu^T]$ is the variance of ν.

Q_C is derived by propagating the uncertainties on the laser readings to the control τ_C.

Expanding τ_C, (27), in Taylor series and taking the expectations at the first order,

$$\begin{array}{l} E[\Delta\tau_C \Delta\tau_C^T] = E[\Delta e_{branch} \Delta e_{branch}^T] + \\ E[\Delta e_{branch} \Delta gs^T] B^T + B E[\Delta gs \Delta gs^T] B^T \end{array} \tag{32}$$

As the stabilization task e_1 on the Voronoï branch and the motion along the branch g_s (27) span orthogonal subspaces, then $E[\Delta e_{branch} \Delta gs^T] \sim 0$, that yields:

$$Q_C = C_{e_{branch}} + B C_{gs} B^T \tag{33}$$

$C_{e_{branch}}$, the covariance of e_{branch}, is determined from (27) with the same covariance propagation rule,

$$C_{e_{branch}} = A C_e A^T + B C_{gs} B^T \tag{34}$$

where C_e is a (2×2) matrix with the variances of the laser readings. The covariance matrix C_{gs}, (3×3), represents the uncertainties related to the motion of the robot along the Voronoï branch, it is approximated by the odometry uncertainty.

The covariance of τ_C, called Q_C, at a bifurcation point is calculated in a similar manner using the equations (28) and yields,

$$\begin{array}{rcl} Q_C & = & C E[\Delta e_{BP} \Delta e_{BP}^T] C^T \\ & = & C C_{e_{BP}} C^T \\ & = & C C_{e_3} C^T \end{array} \tag{35}$$

C_{e_3} is a (3×3) covariance matrix of the laser measurements at a bifurcation point.

The prediction of the relative translation Tr calculated by integrating the desired control input, in (30) and expressed into the frame Xc_k is then:

$$\hat{Tr}_C = R_{\beta_k} \begin{bmatrix} \Delta \hat{x}_C \\ \Delta \hat{y}_C \\ 1 \end{bmatrix} \tag{36}$$

R_{β_k} is a rotation matrix between the frames C_k and Xc_k, figure 7.

The predicted rotation expressed into the frame Xc_k is,

$$\hat{\varphi}_C = \Delta \hat{\theta}_C + \beta_k - \beta_{k+1} \tag{37}$$

and the full predicted motion will be

$$\hat{T}_C = \begin{bmatrix} \hat{Tr}_C \\ \hat{\varphi}_C \end{bmatrix}$$

The covariance $P_{\Delta \hat{X}_C}$ is projected from C_k into Xc_k as,

$$P_{\hat{T}_C} = R_{\beta_k} P_{\Delta \hat{X}_C} R_{\beta_k}^T \tag{38}$$

C. Localization of the robot in the reference frame

Let us consider x_k the estimated position of Xc_k in the reference frame W, and P_{x_k} the associated covariance.

The new estimate x_{k+1} and the new associated covariance $P_{x_{k+1}}$ are calculated by,

1. Merging the two predictions $\hat{T}_L$ and $\hat{T}_C$ of the motion $x_k \rightarrow x_{k+1}$ which were calculated respectively from the correspondence between the local maps I_k and I_{k+1}, described in section IV-A.4, and the integration of the control inputs, described in section IV-B.
2. Mapping the final relative motion expressed in the frame Xc_k into the reference frame W.

The final estimate of the motion RT, $\tilde{T}$, results from the fusion between the two predictions $\hat{T}_L$ and $\hat{T}_C$, as follows,

$$\begin{aligned} \tilde{T} &= P_{\hat{T}_C}(P_{\hat{T}_L} + P_{\hat{T}_C})^{-1}\hat{T}_L + \\ & \quad P_{\hat{T}_L}(P_{\hat{T}_L} + P_{\hat{T}_C})^{-1}\hat{T}_C \end{aligned} \tag{39}$$

and the covariance $P_{\tilde{T}}$:

$$P_{\tilde{T}} = P_{\hat{T}_L}(P_{\hat{T}_L} + P_{\hat{T}_C})^{-1}P_{\hat{T}_C} \tag{40}$$

This robot position, expressed into the reference frame, can be then computed by :

$$x_{k+1} = x_k + R_{\theta_k}\tilde{T} = f(x_k, T) \tag{41}$$

where R_{θ_k} is the rotation matrix between Xc_k and W.

The covariance of x_{k+1} is calculated by updating the uncertainties,

$$\begin{aligned} P_{x_{k+1}} = & \frac{\partial f(x_k,T)}{\partial x} P_{x_k} \frac{\partial f(x_k,T)}{\partial x}^T + \\ & \frac{\partial f(x_k,T)}{\partial T} P_{\tilde{T}} \frac{\partial f(x_k,T)}{\partial T}^T \end{aligned} \tag{42}$$

V. Experimental results

In this section, we present results validating the dead-reckoning method developed in section IV. The results show that such a method improves considerably the localization process as well as the accuracy in the map building during the exploration of the environment.

The test-bed is constituted with the mobile robot ANIS, figure 9, developed in our laboratory[2]. This robot is equipped with a 2D-Laser range-finder with a scanning device that delivers 2000 points of measurements distributed in a 360 degrees scan.

The navigation is performed in an indoor structured but unknown environment as shown in the figure 10.

[2]http://www-sop.inria.fr/icare/icare-fra.html

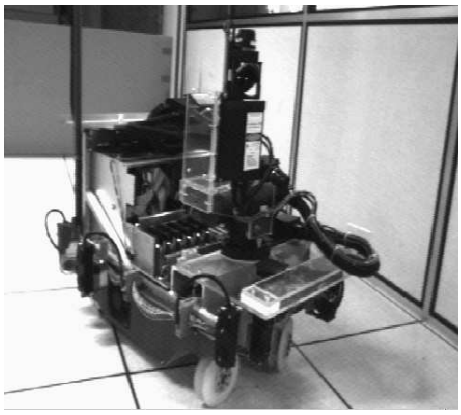

Fig. 9. The robot ANIS.

The robot moves without any reference trajectory or off-line path planning. The trajectories plotted in the figures were calculated and shown just for visualization purpose. The Voronoï graph related to the environment is neither previously known nor calculated during the robot navigation.

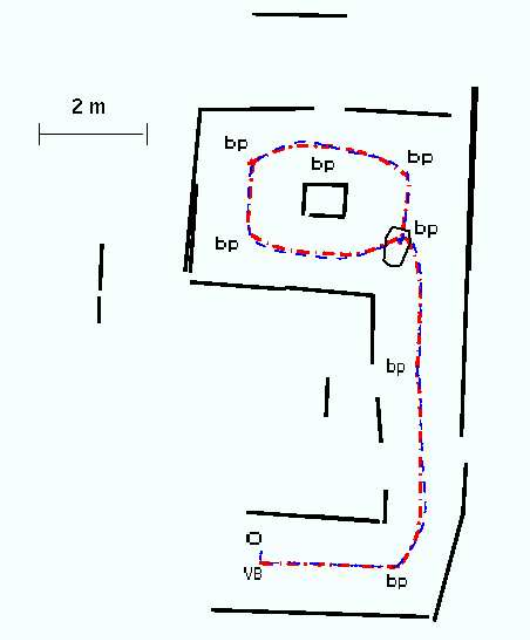

Fig. 10. *Sensor-based navigation, localization and map building.*

The robot starts from the point O, follows the Voronoï branch until it stops at a bifurcation point. Then, it navigates through the successive bifurcation points, marked BP, turning in the clockwise direction around the central object. The localization of the robot with respect to a fixed frame in O is performed when it stops on each BP of the environment. The

current global map of the environment is updated at these points by merging the local scan using an Extended Kalman Filter estimator (Appendix A).

Let us now compare our approach to a classical one uniquely based on odometry. When the robot localization and the map updating are performed only in the bifurcation points, the performances in terms of accuracy and robustness strongly decrease as the distance between two successive bifurcation points grows.

The figure 11 shows what happens when the robot continues the previous navigation task and try to turn back to the starting point. As it can be noted, the estimated robot position diverges when it returns to the initial bifurcation point, at the bottom of the figure. Due to the drift in the estimation of the robot position, a bad matching score is realized between the local and global maps resulting on a distortion as shown in the figure. The results presented in the next sections show that this problem can be avoided when using the motion estimation method described in the section IV. We show in sections V-A and V-B the robustness of the estimation method in a cyclic environment face to unbounded odometry errors, and detail the result obtained in a more large scale environment where the problem of non observability discussed in section IV-A.1 occurs.

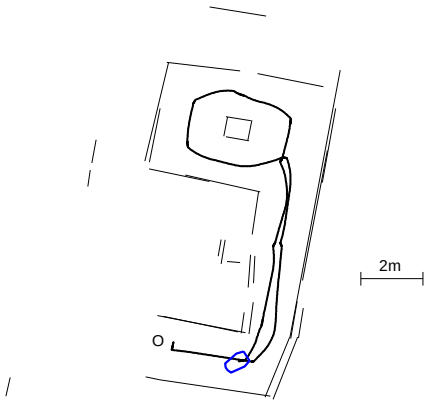

Fig. 11. *Problems occurring with a classical odometry based on wheels encoders data.*

A. Navigating in a cyclic environment

In the figure 12 the robot starts from the point marked by a cross (the starting point of the controlled frame) and a circle (the starting point of the robot's frame) at the left hand side of the figure and goes ahead in the direction of the central box and stops at the first bifurcation point BP. Then, it performs 5 turns around the central box in the clockwise sense for a total distance of $57.73m$. Note that the point of the robot that is stabilized to the BP is the origin of the controlled frame X_c, fixed at the center of the robot as shown in figure 7.

The environment is unknown and the robot explores it with the sensor-based control strategy so that the robot is constrained to move on the Voronoï branches of the environment by the closed loop control laws. The BPs[3] are characteristics of the environment, therefore, due to the sensor-based control scheme, when the robot (or the point X_c) comes back to a BP it converges to a same real position of the environment with a threshold error of $0.03m$ related to the execution of the stabilization task e_3, presented in section III, when the norm of the task e_3 is less than $0.03m$ the robot is considered stabilized at the BP oriented with the arriving branch. These unknown real positions of the robot at each BP of this place are estimated with respect to the constructed local metric map by applying the methodology described in section IV.

The positions of the robot as well as the associated uncertainty ellipses are shown at each BP found during the cyclic motion. The crosses and circles represent the positions of the robot frame, R in figure 7. The odometric positions calculated from the wheel encoders are represented by crosses and the estimated positions given by the estimation method are marked by circles. The estimated BP positions are not represented on the figure 12. As we can see the position estimated by the odometry diverges considerably from the robot real positions at the BPs after some cycles, however the positions estimated by our method perfectly match the real positions of the robot in the environment. The uncertainties associated to the estimated positions are denoted by the ellipses plotted in the BP locations.

When the robot arrives at each BP the estimated position at the end of the branches are used as predictions in the global localization and map building algorithm. This global localization is performed with the fusion of the estimated predictions and the laser measurements using the Extended Kalman Filter (Appendix A).

In the figure 13 the dashed line represents the positions computed by the odometry based on wheel encoders and the dotted one represents the estimated positions provided by our method. We see in this figure

[3]The points equidistants to three segment lines. The minimal distances to these segment lines are extracted from the laser and considered in the stabilization task.

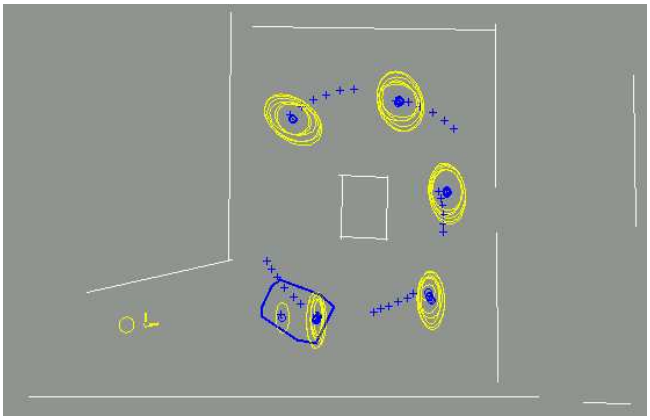

Fig. 12. The robot's behavior in a cyclic environment. The positions of the robot at each BP are shown: the blue crosses correspond to the odometry and the blue circles to the estimations given by our method. The uncertainty ellipses related to the estimated position are shown as well. The environment's map dynamically built during the 7 cycles is equally plo

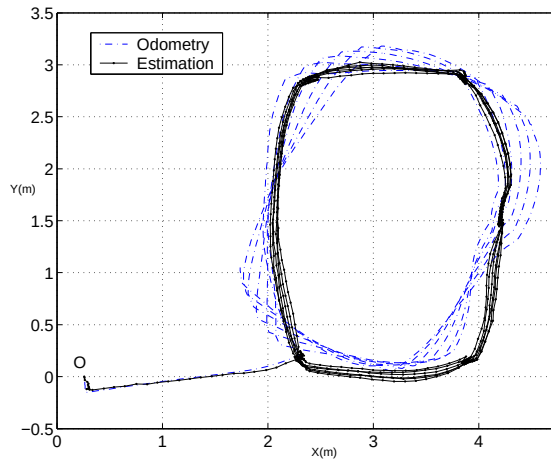

Fig. 13. The trajectories of the xc point of the robot represented into the origin frame fixed in O.

that when the odometry diverges the estimated positions remain close to the real positions of the robot with a bounded error.

When the robot came back to a BP of another place when navigating in a large environment with several places, the fact that the robot came back to a same real position of the environment is used to localize the robot in the global topological model by recognizing the revisited place, which guarantees the fusion between the metric model of different places, as explained in the examples shown in section III.

B. A more largest and significant environment

The navigation in the figure 14 is the same as in the experiment presented in the figure 11. The robot is stabilized to the Voronoï branch starting from an initial position at the point 0, at the bottom of the figure, it explores the possible branches turning around the box in the clockwise sense for returning to the area of the initial position, passing through the bifurcation points in the regions marked C and C'. The experimentation is stopped when the robot returns to the first bifurcation point founded in the region C'. It is shown in the figure 14 that the position estimation errors remain bounded by the application of the motion estimation at the branches as described in the section IV. The precision of the global map generated at the end of the motion is considerably improved.

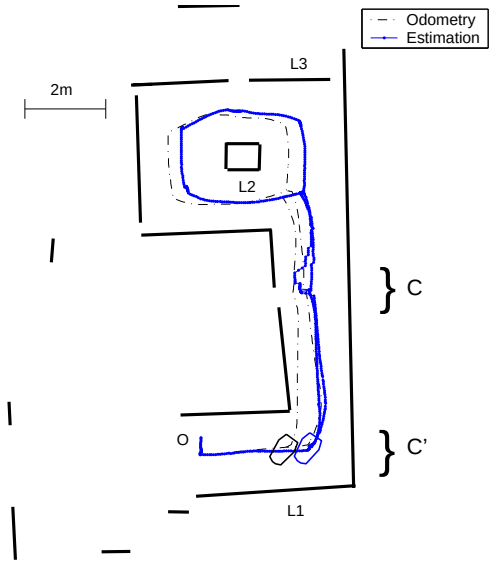

Fig. 14. *Complete navigation with motion estimation. The solid blue line corresponds to the estimated robot positions and the dotted dark line correspond to the odometry data. The global map of the environment constructed up to this point of the navigation is shown as well.*

A zoom in the region C' is shown in the figure 15 where it is noted that the estimated robot position, the solid line, corresponds to the real position of the robot which is stabilized at the bifurcation point of the environment in this region. The dotted line in the figure represents the positions given by the odometry.

The figure 14 illustrates observability problems which can occur when using a motion estimator based on the laser readings only. The estimated positions

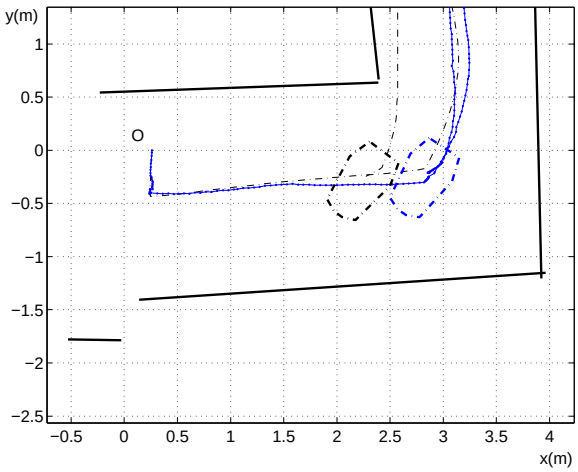

Fig. 15. *A zoom of the region C' of the figure 14. The solid blue line corresponds to the estimated robot positions and the dotted dark line corresponds to the odometric data.*

are unstable around the region C (see the zoom, figure 16) when the robot is navigating in both senses, due to the fact that the translations $\hat{T}r_L$ computed from the laser measurements in this region become not observable. The objects represented by the horizontal lines $L1$, $L2$ and $L3$ of the figure 14 are not perceived by the robot from the region C, the only objects observed from this region are constituted by parallel segments so that the Proposition 1 in the section IV-A.1 is not verified.

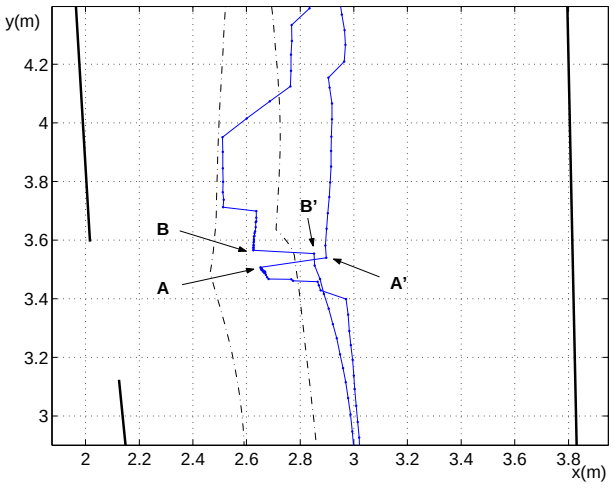

Fig. 16. *A zoom of the region C of the figure 14.*

The results shown in figure 17 are related to a same navigation as in figure 14. The estimates of the robot displacements are computed by (26) in section IV-A.4 with the modifications proposed to handle the relative motions observable. It is noted in the figure that the estimated positions become stable, even when the robot is navigating through the region C.

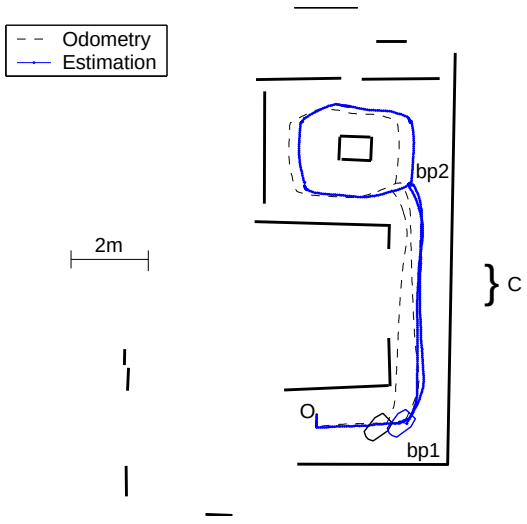

Fig. 17. *Complete navigation with motion estimation. The problem of observability is overpassed using the odometry data to complete the laser observation.*

Finally, the figure 18 illustrates the advantages of merging the robot motion estimations computed from the laser data and the one obtained by integrating the control inputs. In 18.a the estimates of the translations are computed by (25) in section IV-A.4 only from the laser readings and in 18.b with the observable version given by (26). It is only shown the relative motion along the x-axis of the frame C in figure 7, dX, that is the dominant direction of motion is this region. The solid blue lines represents the estimates computed from the laser readings (dXL) and the dashed lines the estimates computed by integrating the velocity control inputs (dXC). The experimentation was performed in good conditions without important slippage on the wheels, so that dXC can be used as a reference, that is not the case with perturbed conditions. In these cases the stability on the estimation dXL is important and it determines the quality of the final fusion between dXC and dXL as described in section IV-C. The results in figure 18 validate the observability issues discussed in sections IV-A.1-IV-A.4.

VI. Conclusions

In the Part-I of this work, we proposed a full sensor-based navigation methodology where feedback control

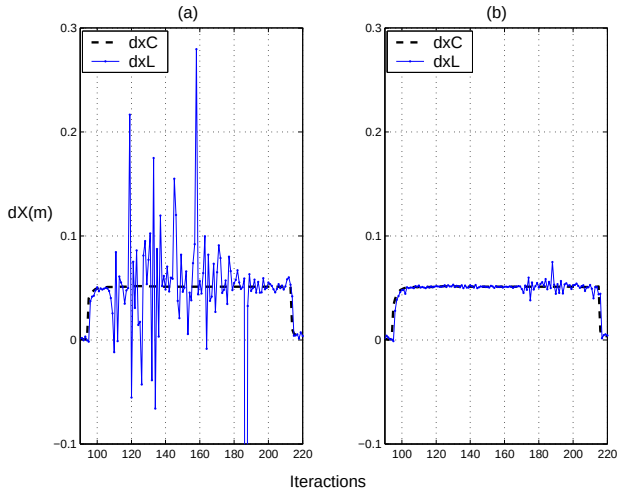

Fig. 18. Estimated relative displacements (a) $\hat{T}r_L$ given by (25) in section IV-A.4; (b) $\hat{T}_L$ given by (26).

laws were derived in such a way that the robot is constrained to move on the Voronoï diagram to explore its free workspace. This methodology is well adapted to the exploration of a corridor-like environment. In this paper, the Part-II of this work, we presented a methodology for localizing the robot and building a representation of the explored environment. In this paper, we focus on the use of a laser range finder providing a planar map of the environment. The use of vision data, which is out of the scope of this paper, in complement to range measurement could of course improve in a large scale the performances and should simplify the problem of identifying the places already visited by the robot, by recognizing corridors, door intersections, etc.

We proposed an hybrid representation of the environment: topological and geometrical, that is built incrementally during the exploration of the environment. The topological model is a direct result of the application of the sensor-based control strategy presented in the Part-I, and represents the connectivity and accessibility of the different regions of the environment. The geometrical model, which is constructed in parallel with the topological one, is a precise description of the robot's free space. The geometrical model was segmented into different places, each place is characterized by a reference frame and a map of line segments, where the robot can be localized with a sufficient precision. The relation and connectivity between the different places of the environment are essentially topological.

The SLAM problem in a place was in particular considered. It was shown that the simultaneous localization and map building (SLAM) results can be considerably improved due to the fact that the robot motions are constrained by feedback control laws. Although the global SLAM result is qualitatively improved with the feedback control methodology it remains limited due to the odometry drift and depends on the distance traveled by the robot between two successive localization and mapping steps.

To overpass this limitation, we proposed a new localization method taking advantage the facts that the relative motion is bounded by feedback control laws and that laser measurements are available at each sampling time. Results were established defining the conditions required for the observability of the robot displacement from the laser readings. Moreover, we have developed a new estimator that provides the displacement of the robot at sampling rate during its motion on the Voronoï branches. This new estimation method merges the estimate of the displacement provided from the laser readings and a prediction computed from the control input.

The proposed control methodology was experimentally validated in our mobile robot. The stability and robustness of the feedback control laws was verified. Experimental results showing the robustness provided by the relative motion estimation method as well as the improvement in the global localization and map building process are presented and discussed.

Appendices

I. Self localization and map building

During the exploration, the robot constructs and updates a rigid metric model composed of a reference frame, sub-frames associated to each BP position and a set of line segments expressed in the reference frame which constitutes the global map , figure A-1.

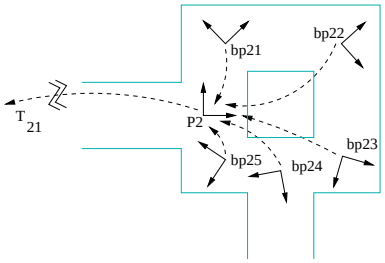

Fig. A-1. *The metric model of the Place 2 of the environment shown in figure 5. $P2$ is the reference frame associated to the place, $BP21$ to $BP25$ are the BP frames rigidly linked to $P2$.*

The simultaneous localization and map building methodology is based on the fusion between the laser range measurements and the dead-reckoning observation using an extended Kalman filter (EKF). The laser

scan (figure 4) is segmented in a set of line segments I_0, computed in the laser frame:

$$I_0 \;=\; \{D_1,\ \ldots,\ D_i,\ \ldots,\ D_n\} \qquad (A.1)$$

where,

$$D_i \;=\; \{P_i,\ Q_i,\ \phi_i,\ \delta_i,\ \sigma^2_{\phi_i},\ \sigma^2_{\delta_i}\} \qquad (A.2)$$

with :
- The end points of the segment $P = [x_p \;\; y_p]$ and $Q = [x_q \;\; y_q]$,
- the line parameters $l = (\delta,\ \phi)$,
- the variances $(\ \sigma^2_{\delta_i},\ \sigma^2_{\phi_i})$ which characterize the segmentation process.

The model of a line segment D_i used in the metric map is shown in figure A-2.

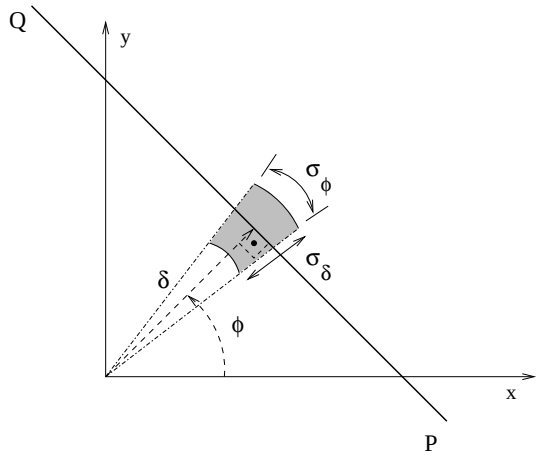

Fig. A-2. Line segment model.

Exploring the place 2, the robot reaches a $BP\ (k{+}1)$ coming from a previous $BP\ (k)$, then the new robot position $X_{k+1} = (x_{k+1}, y_{k+1}, \alpha_{k+1})$ has to be estimated and the global map I_0 expressed in $P2$ has to be updated taken into account the local observation provided by the laser in the $BP\ (k+1)$. The last estimated state $X_{k/k}$ with its associated covariance matrix $P_{k/k}$ of dimension (3×3) is known, the estimation of the new position $(k+1)$ is predicted using the results of the motion estimation method (developed in section IV) applied during the displacement on the branch $k \rightarrow (k+1)$, the prediction is noted $X_{k+1/k}$ with covariance $P_{k+1/k}$. A new set of segments $l^i_{k+1} = (\delta^i_{k+1}, \phi^i_{k+1})$ is extracted from the laser scan, at the $BP\ (k{+}1)$, and constitutes the new observation of the environment I_{k+1}.

A. The observation prediction and matching

Using the current global map of the environment (which is incrementally built at each $BP\ (k)$ in the place reference frame $P2$) and the prediction $X_{k+1/k} = (x_{k+1/k},\ y_{k+1/k}, \alpha_{k+1/k})$ provided by the dead-reckoning method during the displacement of the robot on the branch, we are also able to predict the line segments that are potentially visible from the new robot position at the $BP\ (k+1)$:

$$G(X_{k+1/k}, l_0) \;=\; \begin{bmatrix} d_0 - x_{k+1/k}\cos(\phi_0) - y_{k+1/k}\sin(\phi_0) \\ \phi_0 - \theta_{k+1/k} \end{bmatrix} \qquad (A.3)$$

$I_{k+1/k} = G(X_{k+1/k}, l_0)$ constitutes the prediction of the observation at the $BP\ (k{+}1)$, where $l_0 = (\delta_0, \phi_0)$ is expressed in the reference frame. Then, we can write,

$$I_{k+1} = I_{k+1/k} + E_{k+1} \qquad (A.4)$$

that is the *observation equation* with E_{k+1} the observation error.
The matching between I_{k+1} and $I_{k+1/k}$ is performed by a probabilistic test based on the classical Mahalanobis distance. If the following inequality holds,

$$E_{k+1} S^{-1}_{k+1/k} E^T_{k+1} < \epsilon \qquad (A.5)$$

then, a match occurs between I_{k+1} and $I_{k+1/k}$, where the variable $E_{k+1} S^{-1}_{k+1/k} E^T_{k+1}$ follows a $\mathcal{X}^2$ probability distribution given by tables [1], ϵ is an iso-probability threshold, $S_{k+1/k}$ is the variance of the observation prediction, computed as:

$$S_{k+1/k} = \frac{\partial G}{\partial X_{k+1/k}} P_{k+1/k} \frac{\partial G}{\partial X_{k+1/k}}^{\;T} + R_{k+1} \qquad (A.6)$$

R_{k+1} is the variance matrix of the measurement I_{k+1}.

B. The state estimation

Using the EKF equations, we can now compute the new estimated state and update the covariance matrix at the $BP\ (k+1)$:

$$X_{k+1} = X_{k+1/k} + K_{k+1} E_{k+1} \qquad (A.7)$$

The Kalman gain K_{k+1} is done by,

$$K_{k+1} = P_{k+1/k} \frac{\partial G}{\partial X_{k+1/k}}^{\;T} S^{-1}_{k+1/k} \qquad (A.8)$$

and the covariance of the estimated position is

$$P_{k+1} = (I - K_{k+1} \frac{\partial G}{\partial X_{k+1/k}}) P_{k+1/k} \qquad (A.9)$$

C. Updating the global map by fusion and integration of I_{k+1} elements

Integration of the new segments in the global map I_0

A segment D_i of the local map I_{k+1} that is not matched using (A.5) is added to the global map I_0, after having been projected into the reference frame $P2$, as follows:

$$l'_0 = \begin{pmatrix} \delta'_0 \\ \phi'_0 \end{pmatrix} = \begin{bmatrix} \delta_{(k+1)} + xc(\Phi) + ys(\Phi) \\ \Phi \end{bmatrix}$$
$$l'_0 = \mathcal{M}(X_{(k+1)/(k+1)},\ l_{(k+1)})$$

where l_{k+1} is computed on the estimated position $X_{k+1/k+1} = \{x,\ y,\ \theta\}$ and $\Phi = \phi_{(k+1)} + \theta$

The covariances associated to the projected line l'_0 are calculated by linearizing the nonlinear system (A.10) around the mean values $l'_0 = (\delta'_0\ \phi'_0)^T$:

$$\Delta p'_0 = Jm_x \Delta X_{(k+1)/(k+1)} + Jm_l \Delta l_{(k+1)} \quad \text{(A.10)}$$

where :

$$Jm_x = \frac{\partial \mathcal{M}}{\partial X_{(k+1)/(k+1)}}$$
$$Jm_l = \frac{\partial \mathcal{M}}{\partial l_{(k+1)}}$$

and the covariance matrix is given by :

$$\begin{aligned} C'_0 &= E[\Delta l'_0 \Delta {l'_0}^T] \\ C'_0 &= Jm_x P_{(k+1)/(k+1)} Jm_x^T + Jm_l C_{(k+1)} Jm_l^T \end{aligned}$$

where,

$$C_{(k+1)} = \begin{bmatrix} \sigma^2_{\delta_{(k+1)}} & 0 \\ 0 & \sigma^2_{\phi_{(k+1)}} \end{bmatrix}$$

assuming $E[\Delta l'_0 \Delta {X_{(k+1)/(k+1)}}^T] = 0$.

The end points of segment D_i in the local map I_{k+1}, $q_{(k+1)}$, are projected into the reference frame $P2$ by the transformation:

$$q'_0 = \begin{pmatrix} x \\ y \end{pmatrix} + \begin{bmatrix} cos(\theta) & -sin(\theta) \\ sin(\theta) & cos(\theta) \end{bmatrix} q_{(k+1)} \quad \text{(A.11)}$$

where $X_{k+1/k+1} = \{x,\ y,\ \theta\}$ is the estimated position.

Then, a new element $D_j = \{q'_0,\ l'_0,\ C'_0\}$ is integrated to the metric map of the place I_0 represented on the reference frame $P2$.

Fusion between the matched segments

The fusion of the couples of segment lines of I_0 and I_{k+1}, represented by its line parameters l_0 and $l_k + 1$, which were matched thanks to the test (A.5) is performed as follows. The end points of all the segments that contributed to the construction of the line l_0 are stored in a list of points, this list is augmented by the integration of the new end points of $l_k + 1$ after having been projected into the reference frame $P2$ using (A.11). A polygonal segmentation is then performed in this list of end points associated to l_0 and the estimation of the line parameters are updated. The covariances of these new parameters result from the segmentation process. New end points for the new l_0 are extracted from the augmented list of points. In this way, at the position $BP\ (k+1)$ the segment l_0 is updated with the fusion of its correspondent segment $l_(k+1)$.

II. Development of the equation (24) of the section IV-A.4

The covariance of the predicted relative motion $\hat{Tr}_L$ calculated in section IV-A.4 is given by:

$$C_{\hat{Tr}_L} = E[\Delta Tr \Delta Tr^T]$$

where ΔTr is given from the equation (23) as:

$$\Delta Tr = -(\sum_{l=1}^{nc} a_l)^{-1} \sum_{l=1}^{nc} p_l \Delta M_l$$

where:

$$\begin{aligned} a_l &= \mu_l \tfrac{\partial f}{\partial Tr}|_{(\hat{Tr}_L, \hat{M}_l)} \\ p_l &= \mu_l \tfrac{\partial f}{\partial M_l}|_{(\hat{Tr}_L, \hat{M}_l)} \end{aligned}$$

Developing the expectation $E[\Delta Tr \Delta Tr^T]$,

$$E[\Delta Tr \Delta Tr^T] = E[(\sum_{l=1}^{nc} a_l)^{-1} (\sum_{l=1}^{nc} p_l \Delta M_l) \cdot (\sum_{l=1}^{nc} p_l \Delta M_l)^T (\sum_{l=1}^{nc} a_l)^{-T}] =$$
$$(\sum_{l=1}^{nc} a_l)^{-1} E[(\sum_{l=1}^{nc} p_l \Delta M_l)(\sum_{l=1}^{nc} p_l \Delta M_l)^T] (\sum_{l=1}^{nc} a_l)^{-T}$$

the expectation $E[(\sum_{l=1}^{nc} p_l \Delta M_l)(\sum_{l=1}^{nc} p_l \Delta M_l)^T]$ is calculated as follows,

$$E[(\sum_{l=1}^{nc} p_l \Delta M_l)(\sum_{l=1}^{nc} p_l \Delta M_l)^T] =$$
$$E[(\sum_{l=1}^{nc} p_l \Delta M_l \Delta M_l^T p_l^T) + p_l \Delta M_l \sum_{j=1,\ j \neq l}^{nc} \Delta M_j^T p_j]$$

considering $E[\Delta M_l \Delta M_j^T] = 0$ if $(j \neq l)$ then,

$$E[(\sum_{l=1}^{nc} p_l \Delta M_l)(\sum_{l=1}^{nc} p_l \Delta M_l)^T] = \sum_{l=1}^{nc} p_l E[\Delta M_l \Delta M_l^T] p_l^T$$

and,

$$C_{\hat{Tr}_L} = (\sum_{l=1}^{nc} a_l)^{-1} \sum_{l=1}^{nc} p_l E[\Delta M_l \Delta M_l^T] p_l^T (\sum_{l=1}^{nc} a_l)^{-T}$$
$$= (\textstyle\sum_{l=1}^{nc} a_l)^{-1} \{\sum_{l=1}^{nc} p_l C_{M_l} p_l^T\} (\sum_{l=1}^{nc} a_l)^{-T}$$

References

[1] Ayache, N. "Construction et Fusion de Reprsentations Visuelles 3D", *Thse d'tat*, Universit de Paris-sud, 1988.

[2] Bandera, A., Urdiales, C., Sandoval, F. "An hierarchical approach to grid-based and topological maps integration for autonomous indoor navigation", *Proc. IEEE/RSJ International conference on intelligent robots and systems (IROS'2001)*, Maui, Hawaii, USA, 2001.

[3] P.Bonnifait, G.Garcia, "Design and Experimental Validation of an Odometric and Goniometric Localization System for Outdoor Robot Vehicles", *IEEE Trans. on Rob. and Automation*, vol. 14, no. 4, pp. 541-548, Aug. 1998.

[4] G.A.Borges, M.-J.Aldon, T.Gil. "An optimal pose estimator for map-based mobile robot dynamic localization: Experimental comparison with the EKF", *Proc. IEEE Int. Conf. Robotics and Automation*, Seoul, Korea, May 2001.

[5] Bailey, T., Nebot, E. "Localization in large-scale environments", *Robotics and autonomous systems*, vol. 37, pp. 261-281, 2001.

[6] Chatila, R., Laumond, J.P. "Position referencing and consistent world modeling for mobile robots", *Proc. IEEE Int. Conf. on robotics and automation*, pp. 138-145, 1985.

[7] H.Choset, K.Nagatani. "Topological simultaneous localization and mapping (SLAM): toward exact localization without explicit localization",*IEEE Transactions on Robotics and Automation*, vol.17, no. 2, p. 125-137, April 2001.

[8] J.L.Crowley, "World Modeling and Position Estimation for a Mobile Robot Using Ultrasonic Ranging". *Proc. IEEE Int. Conf. Robotics and Automation*, pp.674-680, 1989.

[9] H.F.Durrant-Whyte, J.J.Leonard,"Direct Sonar Sensing for Mobile Robot Navigation". *Kluwer Academic Publishers*, 1992.

[10] H.J.S.Feder,J.J.Leonard,C.M.Smith, "Adaptive Mobile Robot Navigation and Mapping", *The Int. Journal of Rob. Research*, v.18, n.7, pp. 650-668, July 1999.

[11] Franz, M.O., Scholkopf, B., Mallot, H.A., Bulthoff, H.H. " Learning view graphs for robot navigation", *Autonomous Robots*, vol. 5, no. 1, pp. 111-125, 1998.

[12] Gaspar, J., Winters, N., Santos-Victor, J. "Vision-based navigation and environmental representations with an omnidirectional camera", *IEEE Transactions on robotics and automation*, vol. 16, no. 6, pp. 890-898, 2000.

[13] P.Hébert, S.Betgé-Brezetz, R.Chatila, "Decoupling Odometry and Exteroceptive Perception in Building a Global World Map of a Mobile Robot: The Use of Local Maps". *Proc. IEEE Int. Conf. of Robotics and Automation*, pp. 757-764, 1996.

[14] K.Konolige. "Improved occupancy grids for map building", *Autonomous Robots*, vol.4, no.4, pp.351-367, Oct. 1997.

[15] Kuipers, B., Byun, Y.T., "A robot exploration and mapping strategy based on semantic hierarchy of spatial representations", *Robotics and autonomous systems*, vol. 8, no. 1-2, pp. 47-63, 1991.

[16] L.Matthies, A.Elfes. "Integration of Sonar and Stereo Range Data Using a Grid-Based Representation", *Proc. IEEE Int. Conf. of Robotics and Automation*, pp. 727-733, 1988.

[17] P.Moutarlier, R.G.Chatila. "Stochastic multisensory data fusion for mobile robot location and environment modelling", In *Proc. International Symposium on Robotics Research*, pp. 85-94, Tokyo, 1989.

[18] K.Nagatani, H.Choset, "Toward robust Sensor-Based Exploration by Constructing Reduced Generalized Voronoï Graph", *Proc. IEEE/RSJ Int. Conf. on Intelligent Robots and Systems(IROS'99)*, v.3, pp. 1687-1692, 1999.

[19] H.Nijmeijer, A.Schaft."Nonlinear dynamical control systems",*Springer*, 467p., 1990.

[20] D.Pagac, E.M.Nebot, H.F.Durrant-Whyte. "An Evidential Approach to Map-Building for Autonomous Vehicles", *IEEE Transactions on Robotics and Automation*, vol. 14, no.4, pp. 623-629, Aug. 1998.

[21] R.C.Smith, P.Cheeseman, "On the Representation and Estimation of Spatial Uncertainty", *Int. Journal of Robotics Research*,vol. 5, No. 4, pp. 56-68, 1986.

[22] Thrun, S. "Learning metric-topological maps for indoor mobile robot navigation", *Artificial Intelligence*, vol. 99, pp. 21-71, 1998.

[23] Ulrich, I., Nourbakhsh, I. "Appearance-based place recognition for topological localization", *Proc. IEEE International Conference on Robotics and Automation*, pp. 1023-1029, 2000.

[24] A.C.Victorino, P.Rives, J.-J.Borrelly. "Localization and Map Building Using a Sensor-Based control Strategy", in *Proc. IEEE/RSJ Int. Conf. on Intelligent Robots and Systems(IROS)*, Takamatsu, Japan, 2000.

[25] A.C.Victorino, P.Rives, J.-J.Borrelly, "A Relative Motion Estimation by Combining Laser Measurement and Sensor-Based Control". *Proc. IEEE Int. Conf. on Robotics and Automation(ICRA'2002)*, Washington-DC, USA, May 2002.

[26] A.C.Victorino, P.Rives, J.-J.Borrelly. "A Relative Motion Estimation Using a Bounded Error Method", in *Proc. IEEE/RSJ Int. Conf. on Intelligent Robots and Systems(IROS)*, Lausanne, Swiss, October 2002.